



Investigation of the effects of nonstationary features on rock joint roughness using the laser scanning technique

Yunfeng Ge¹ · Zishan Lin¹ · Huiming Tang^{1,2} · Binbin Zhao³ · Hongzhi Chen¹ · Zhiguo Xie¹ · Bin Du¹

Received: 22 May 2019 / Accepted: 17 February 2020 / Published online: 4 March 2020
© Springer-Verlag GmbH Germany, part of Springer Nature 2020

Abstract

Accurately estimating rock joint roughness is crucial for understanding the shear mechanism and permeability behavior of a rock mass. Several influencing factors, including anisotropy, measurement noise, and the scale effect and sampling interval, have been considered. However, little attention is paid to the influences of nonstationary features on the roughness assessment. In this study, a portable laser scanner was employed to collect high-density 3D point clouds of ten natural rock joint specimens. Based on two parameters, namely, the bright area percentage (*BAP*) and $\theta_{\max}^*/(C + 1)$, where θ_{\max}^* is the maximum apparent dip angle and *C* is a dimensionless fitting parameter, the rock joint roughness was determined before and after removing nonstationary features, and a comparison showed that nonstationary features have a considerable influence on the roughness. Subsequently, an approach was proposed to remove nonstationary features through the conversion of spatial coordinates, and an application to a roughness evaluation illustrated that similar trends are observed between the *BAP* and $\theta_{\max}^*/(C + 1)$ with respect to the point clouds of ten rock joints whose nonstationary features were removed. These findings reveal that nonstationary features should be removed to improve the accuracy and comparability of the roughness assessments.

Keywords Rock joint · Roughness estimation · Nonstationary features · 3D laser scanning

Introduction

Acquiring a rock joint roughness estimate contributes to a better understanding of the failure mechanism, hydraulic properties, and permeability characteristics of a rock mass (Tang et al. 2019; Tse and Cruden 1979). To date, a number of approaches have been suggested to determine the rock joint

roughness, including the joint roughness coefficient (*JRC*) (Barton 1973; Barton and Choubey 1977), the mathematical statistics (Wu and Ali 1978; Maerz et al. 1990; Belem et al. 2000), and the fractal dimension (Clark 1986; Turk et al. 1987; Odling 1994; Xie et al. 1998; Babanouri et al. 2013). Meanwhile, with the rapid development of surveying and mapping technologies, noncontact measurements, such as 3D laser scanning, have been widely used to evaluate rock joint roughness by capturing high-density point clouds, and several successful investigations have demonstrated the high resolution and efficiency of laser scanning technology (Kulatilake et al. 1995; Mlynarczuk 2010; Jiang et al. 2016; Mah et al. 2016; Nizametdinov et al. 2016; Ge et al. 2017). Furthermore, to assess the rock joint roughness more accurately, error analyses have been conducted by a large number of scholars while taking the influences of the sampling direction (Du and Tang 1993; Tatone and Grasselli 2010), sampling scale (Ge et al. 2010; Luo et al. 2015), sampling interval (Yu and Vayssade 1991; Ge et al. 2014), and range measurement noise (Khoshelham et al. 2011; Bitenc et al., 2016) into account. Natural rock joints are composed of both stationary and nonstationary components (Fig. 1). Stationary components are mainly associated with the surface morphology of rock joints,

Highlights

- (1) The effects of nonstationary features on rock joint roughness were investigated.
- (2) An approach for removing the nonstationary features of a rock joint was proposed.

✉ Huiming Tang
tanghm@cug.edu.cn

- ¹ Faculty of Engineering, China University of Geosciences, Wuhan 430074, China
- ² Three Gorges Research Center for Geo-hazard, Ministry of Education, China University of Geosciences, Wuhan, Hubei, China
- ³ Research Institute of Transmission and Transformation Projects, China Electric Power Research Institute Co., Ltd, State Grid Corporation of China, Beijing, China

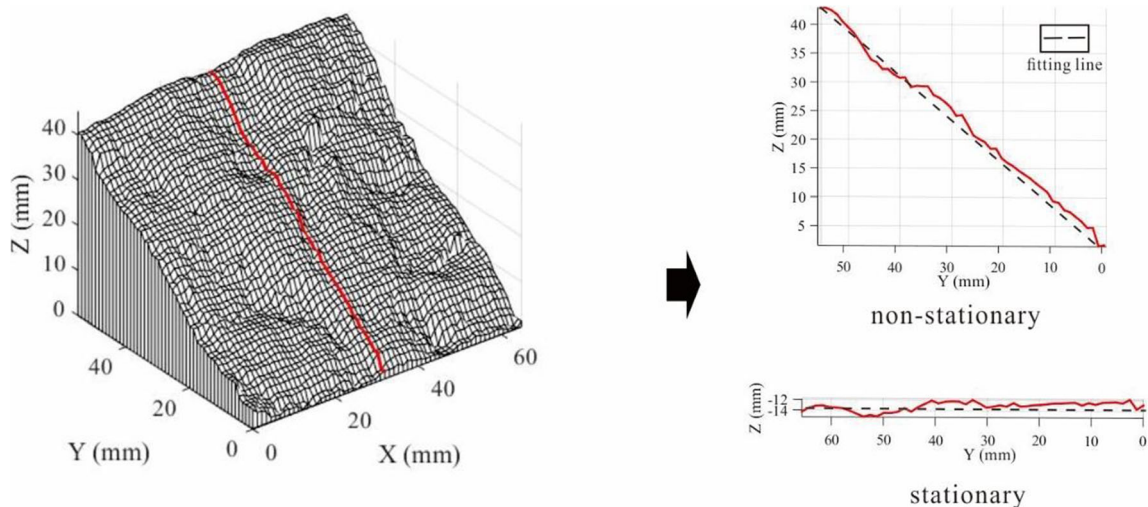


Fig. 1 Definitions of the stationary and nonstationary components of rock joint roughness at the 2D level

whereas nonstationary components represent the global trend of rock joint morphology.

Some attempts have been made to describe and observe the nonstationary features of rock joint roughness. Li et al. (2018) considered the waviness with the highest amplitude along the shear direction to quantitatively describe the nonstationary features of rock joints and evaluated the effect of this waviness on the shear behavior of rock joints under a constant normal stiffness. Kulatilake et al. (1995, 2006) suggested that the average inclination angle I along the considered direction can characterize the nonstationarity of rock joint roughness. Similarly, Jiang et al. (2016) employed the basic roughness angle φ_0 to quantify structural nonstationary components. Unfortunately, at present, insufficient research has been performed on the effects of nonstationary features on rock joint roughness, and thus, an adequate method for removing such features during a roughness estimation is currently lacking.

The objectives of our work are to study the effects of nonstationary features on rock joint roughness and to propose an approach to remove these features of rock joints, thereby improving the accuracy of roughness estimates.

Collection of rock joint specimens point clouds

In this study, a 3D OKIO-FreeScan X5 laser scanner, manufactured by Tianyuan 3D, was employed to capture point clouds of 10 rock joint specimens, which were collected from a quartz sandstone in the Jurassic Suini Group (J_3s) within the Majiagou landslide region in Zigui County, Yichang City, Hubei Province, China. The range of operation of the laser scanner is 30×25 cm with a maximum resolution of 0.05 mm at a distance of 30 cm. This portable laser scanner is also

characterized by a high speed (350,000 points/s) and a light weight (0.95 kg), as it was designed to be small and easy to operate within a laboratory; consequently, it can be controlled by a laptop through a connected communication cable (Fig. 2). Occluded areas, that is, areas in which no points are captured, will be generated when the line of sight is parallel to the joint surface morphology at certain angles (Ge et al. 2018). Therefore, to collect point clouds of specimens without missing data, multiple individual measurements from different angles and positions are required. These individual measurements can be transformed into a uniform coordinate system by affixing several target points, which are automatically recognized based on their relative position around the rock joint specimen, with a diameter of 3 mm. Accordingly, the LED brightness was set at 550 and the laser intensity was established at 600, mainly based on the specimen color. To capture more information about the topography of the rock joint surface, the scanning interval was specified as 0.05 mm, leading to a high density of points (approximately



Fig. 2 Configuration of the portable laser scanning system

2,000,000~3,000,000) produced for each specimen. More details regarding the scanning tests are summarized in Table 1. In this manner, the point clouds generated by laser scanning are consistent with the physical surfaces of the rock joints based on the morphology illustrated in Fig. 3.

Influences of nonstationary features on rock joint roughness

The effects of nonstationary features on rock joint roughness were investigated based on qualitative analysis and laboratory work.

Qualitative analysis

Barton (1973; 1977) provided ten standard profiles without nonstationary components to characterize rock joint roughness and proposed an empirical formula to estimate the peak shear strength of rock joints that is well-known as the *JRC-JCS* model:

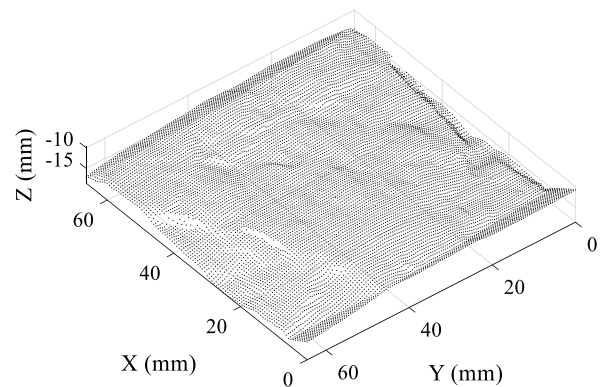
$$\tau_p = \sigma_n \cdot \tan \left[\phi_b + JRC \cdot \lg \left(\frac{JCS}{\sigma_n} \right) \right] \quad (1)$$

where τ_p is the peak shear strength, σ_n is the normal stress, *JRC* indicates the joint roughness coefficient, *JCS* represents the joint compression strength, and ϕ_b is the basic friction angle obtained from residual shear tests on flat unweathered rock discontinuities.

By definition, the *JRC*, which is used to represent rock joint roughness, can be determined according to the profiles without nonstationary features, and ϕ_b , which is independent of the *JRC*, has a close relation to the global trend (nonstationary features). That is, *JRC* captures the stationary components of rock joint roughness, while ϕ_b captures the nonstationary components. Hence, a roughness estimation should be performed based on rock joint profiles or surfaces without nonstationary features.



(a)



(b)

Fig. 3 Comparison between **a** a rock joint surface and **b** the corresponding point cloud

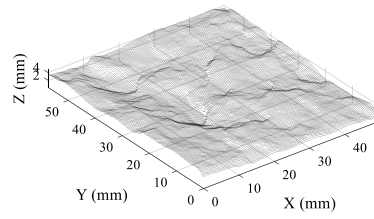
On the other hand, the generation of some deviation is inevitable when preparing specimens and collecting data from rock joints, and this deviation results in the introduction or enlargement of nonstationary features. During specimen preparation, it is difficult to fully preserve the spatial status of rock joints in situ;

Table 1 Summary of the scanning parameters for the 10 rock joint specimens

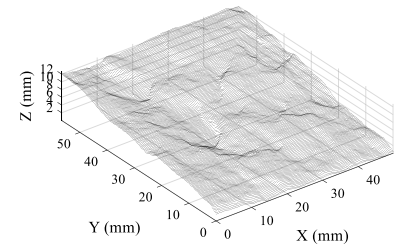
Joint ID	Scale (mm × mm)	Sampling interval (mm)	LED brightness	Laser intensity	Points count
FSS-1D	60 × 60	0.05	550	600	2,223,838
FSS-1 U	65 × 63				2,525,502
M1-5D	65 × 65				2,635,762
M1-5U	65 × 65				2,614,310
M2-1D	63 × 63				2,467,504
M2-1U	68 × 68				2,929,087
MS1-4D	70 × 65				2,666,412
MS1-4U	65 × 65				2,745,065
S1-2D	65 × 65				2,850,452
S1-2U	65 × 65				2,682,775



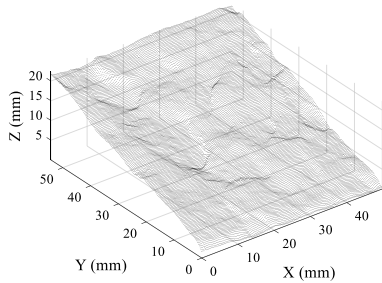
(a)



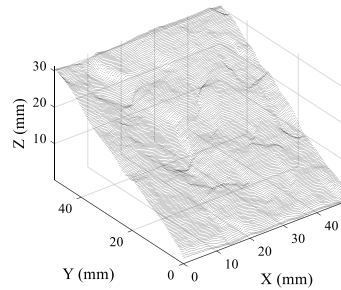
(b)



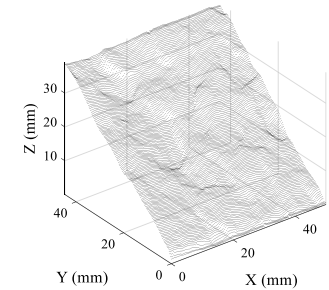
(c)



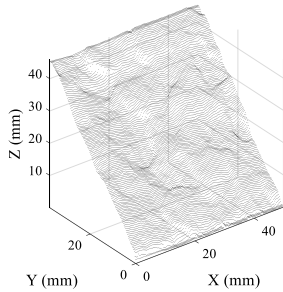
(d)



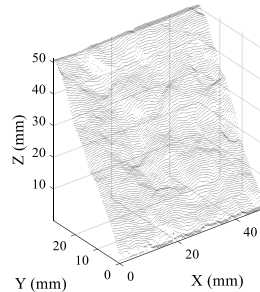
(e)



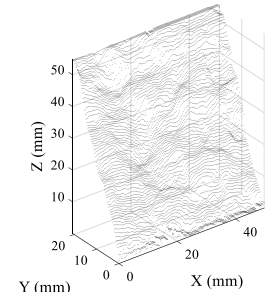
(f)



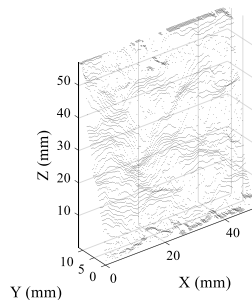
(g)



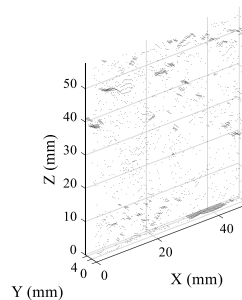
(h)



(i)



(j)



(k)

Fig. 4 Variability of point clouds with different inclination angles: **a** rock joint specimen S1-2U; **b** inclination angle = 0°; **c** inclination angle = 10°; **d** inclination angle = 20°; **e** inclination angle = 30°; **f** inclination angle =

40°; **g** inclination angle = 50°; **h** inclination angle = 60°; **i** inclination angle = 70°; **j** inclination angle = 80°; **k** inclination angle = 90°

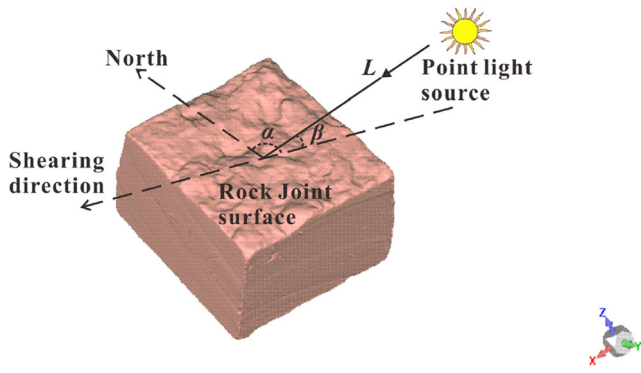


Fig. 5 Schematic diagram of the BAP algorithm

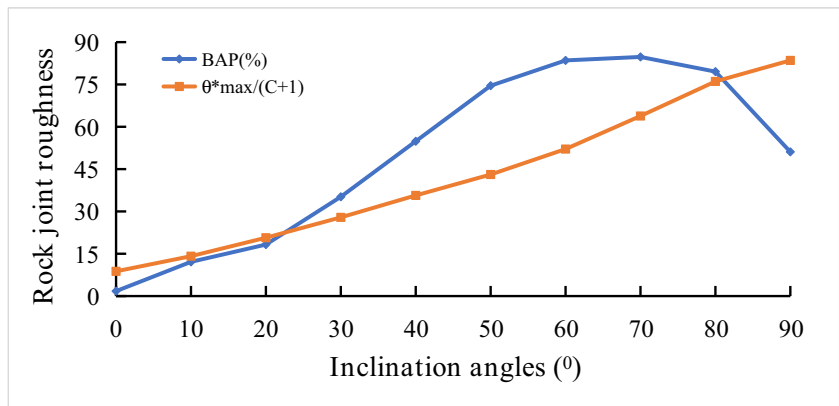
this spatial status always has more influence on the nonstationary components than on the stationary components. Moreover, a similar issue is encountered in the profile construction or surface acquisition of rock joints. For example, the laser scanner used in this study lacks an absolute coordinate system during the collection of the point clouds, and thus, the 3D point clouds are represented in a local coordinate system. Additionally, it is impossible to place the rock joint specimens on an absolute horizontal plane. Therefore, some errors related to nonstationary features are produced when specifying a local coordinate system for point clouds. This is the reason why some rock joint point clouds are oriented with a large inclination angle, as discussed in the next subsection.

This qualitative analysis demonstrates that a rock joint roughness estimation should be performed without considering nonstationary features that are liable to be produced during data collection and lead to an inaccurate assessment. To ensure that the data are comparable, a roughness evaluation of rock joints should be conducted under stationary conditions. In other words, when evaluating rock joint roughness, nonstationary features should be removed.

Laboratory work

To quantifiably estimate the effects of nonstationary features on rock joint roughness, a series of point clouds with various

Fig. 6 Variance of the BAP and $\theta^*_{max}/(C + 1)$ with different nonstationary features



inclination angles ranging from 0° to 90° were produced by placing a joint specimen on an inclined plane with the corresponding slope (Fig. 4). Two indexes, namely, the bright area percentage (BAP) and $\theta^*_{max}/(C + 1)$, were calculated to quantify the roughness of rock joints with different nonstationary features.

According to laboratory observations, steeply dipping facets, facing to the shear direction, have been widely recognized to possess more opportunities to maintain contact and contribute more to residence during rock joint shear failure (Grasselli and Egger 2003; Ge et al. 2017). In the BAP method, these potential contact facets can be detected from point clouds based on their brightness under the illumination of an artificial light source (Fig. 5). The brightness of a facet varies with its dip direction and dip angle, and facets with higher brightness values are the required miniscule planes. The BAP value can be determined by the ratio of the area of brighter facets (P_b) to the total area of the rock joint surface (P_t), as written in Eq. (2) (Ge et al. 2015):

$$BAP = P_b/P_t \times 100\% \tag{2}$$

Similarly, these potential contact areas are closely related to the minimum apparent dip angle of the facets, and their relationship can be described as follows:

$$A_{\theta^*} = A_0 \left(\frac{\theta^*_{max} - \theta^*}{\theta^*_{max}} \right)^C \tag{3}$$

where A_{θ^*} is the potential contact area, A_0 is the peak value of the potential contact area, θ^* is the minimum apparent dip angle, θ^*_{max} denotes the maximum apparent dip angle of the facets, and C is a dimensionless fitting parameter. $\theta^*_{max}/(C + 1)$ is always chosen to characterize the roughness of a rock joint (Grasselli and Egger 2003; Tatone and Grasselli 2009).

Figure 6 shows the rock joint roughness variability with different inclination angles based on the BAP and $\theta^*_{max}/(C + 1)$ algorithms. Evidently, nonstationary features have

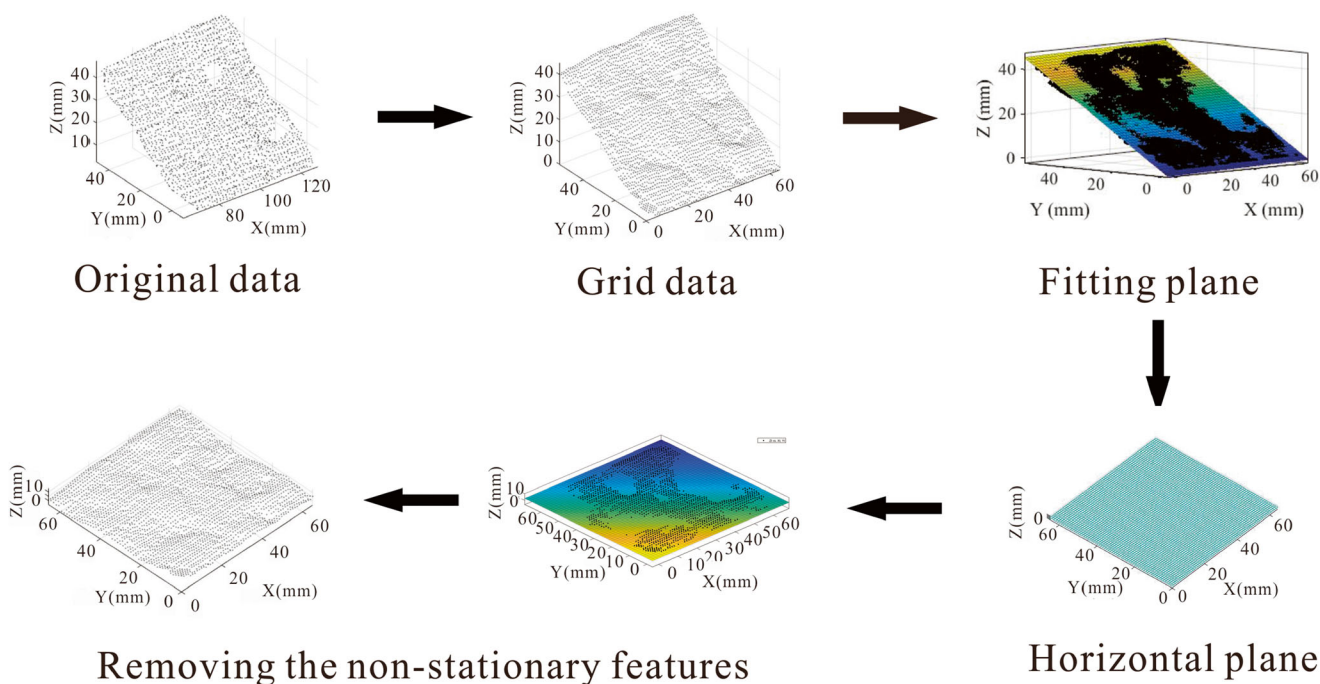


Fig. 7 Illustration of the proposed algorithm for removing the nonstationary features of rock joints

significant impacts on the roughness assessment. There are two distinctly different trends in the roughness estimation. $\theta_{\max}^*/(C+1)$ gradually increases with an increase in the inclination angle, while the *BAP* grows with the inclination angle and peaks at an inclination angle of 70° , followed by a reduction. More remarkably, the difference between the *BAP* and $\theta_{\max}^*/(C+1)$ increases with an increasing inclination angle, and the extent of the effect is proportional to the inclination angle.

Methodology for removing nonstationary features

Based on the abovementioned investigation, a sufficient rock joint roughness estimation accuracy can be achieved only from a point cloud without nonstationary features. Assume that P is a source point cloud with nonstationary features and that Q is the target point cloud without nonstationary features. Nonstationary features can be removed in the process of converting P into Q using a rotation matrix R and a translation vector T . Their relationship can be given by the following:

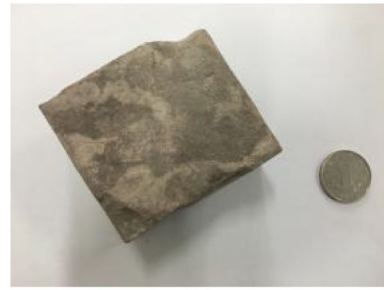
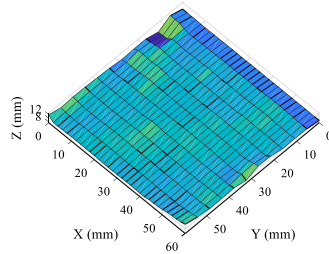
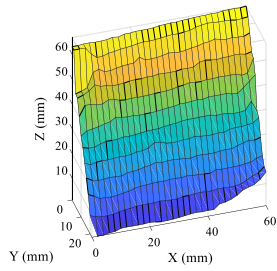
$$Q = P \cdot R + T \quad (4)$$

The goal of removing nonstationary features is to find R and T , which can be determined using minimum iterative errors (e.g., the iterative closest point (*ICP*) algorithm) and feature-based methods (Ma et al. 2017). However, Q is uncertain in our case, and the above algorithms are difficult to apply

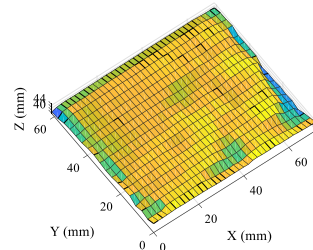
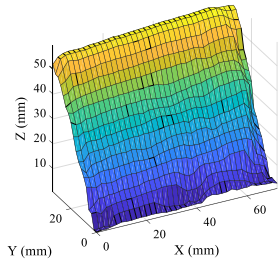
to determine the R and T . Therefore, this paper presents a method for removing the nonstationary feature direction. The procedure is subdivided into five steps (Fig. 7):

- (1) Creating the grid data: the original point clouds, which are captured by a laser scanner with an irregular interval, are converted into grid data where the points are linearly spaced using an interpolation algorithm, making the processing and retrieval of data more efficient.
- (2) Fitting the plane to the points: the multiple linear regression method of least squares is adopted to establish the fitting plane of the point cloud of rock joints.
- (3) Determining the distance and dimension of the point clouds: the distances from all points to the aforementioned fitting plane are calculated and stored. The shapes of the rock joint specimens are rectangles, and their lengths and widths are estimated by spatial queries in the point cloud grid data.
- (4) Generating the horizontal plane: a horizontal plane (*XY* plane) is created at the same dimension as a rock joint specimen and discretized into numerous finite element meshes with the same interval as the grid data of the point cloud.
- (5) Removing the nonstationary features: new point clouds are produced at the nodes of the mesh model with Z

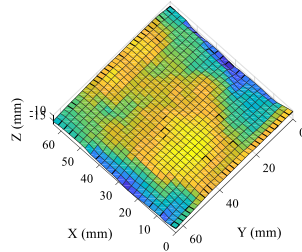
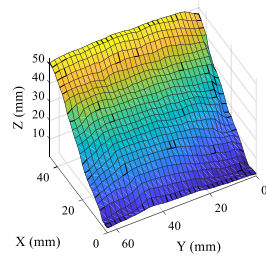
Fig. 8 Comparison of the roughness estimates from before and after removing the nonstationary features of 10 rock joint specimens (for clarity, coarsely gridded data with an interval of 2 mm are used for visual observation; however, fine data on a grid of 0.03×0.03 mm were used in the calculation)



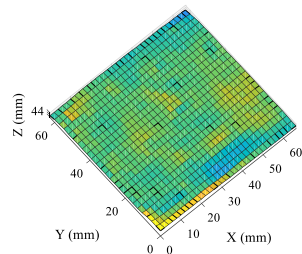
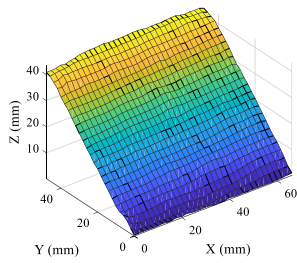
(a) FS5-1D



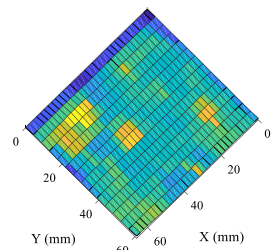
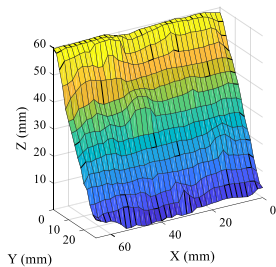
(b) FS5-1U



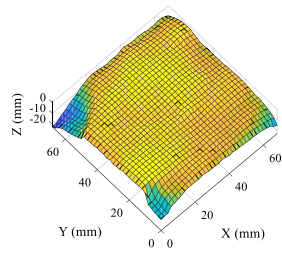
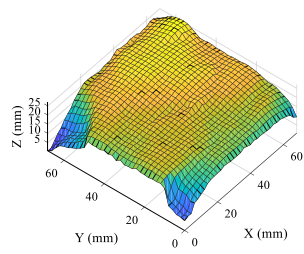
(c) M1-5D



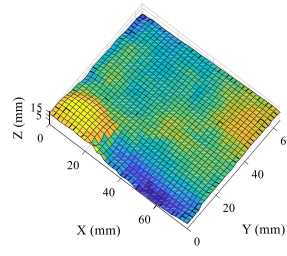
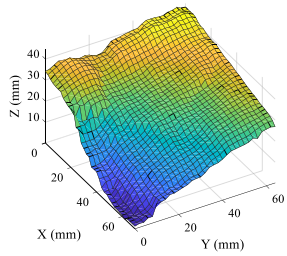
(d) M1-5U



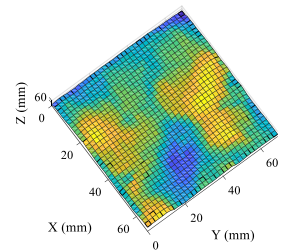
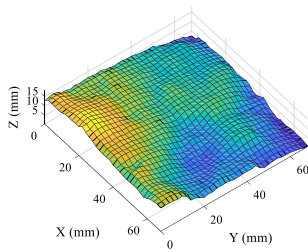
(e) M2-1D



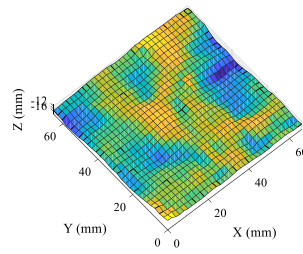
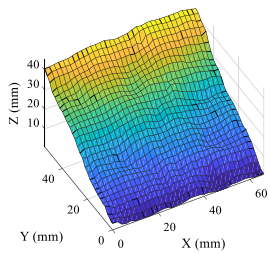
(f) M2-1U



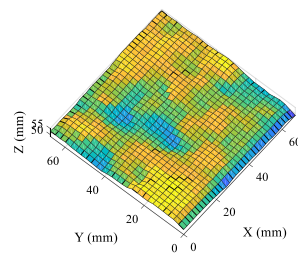
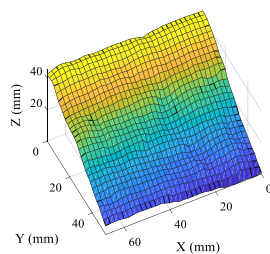
(g) MS1-4D



(h) MS1-4U



(i) S1-2D



(j) S1-2U

Fig. 8 continued.

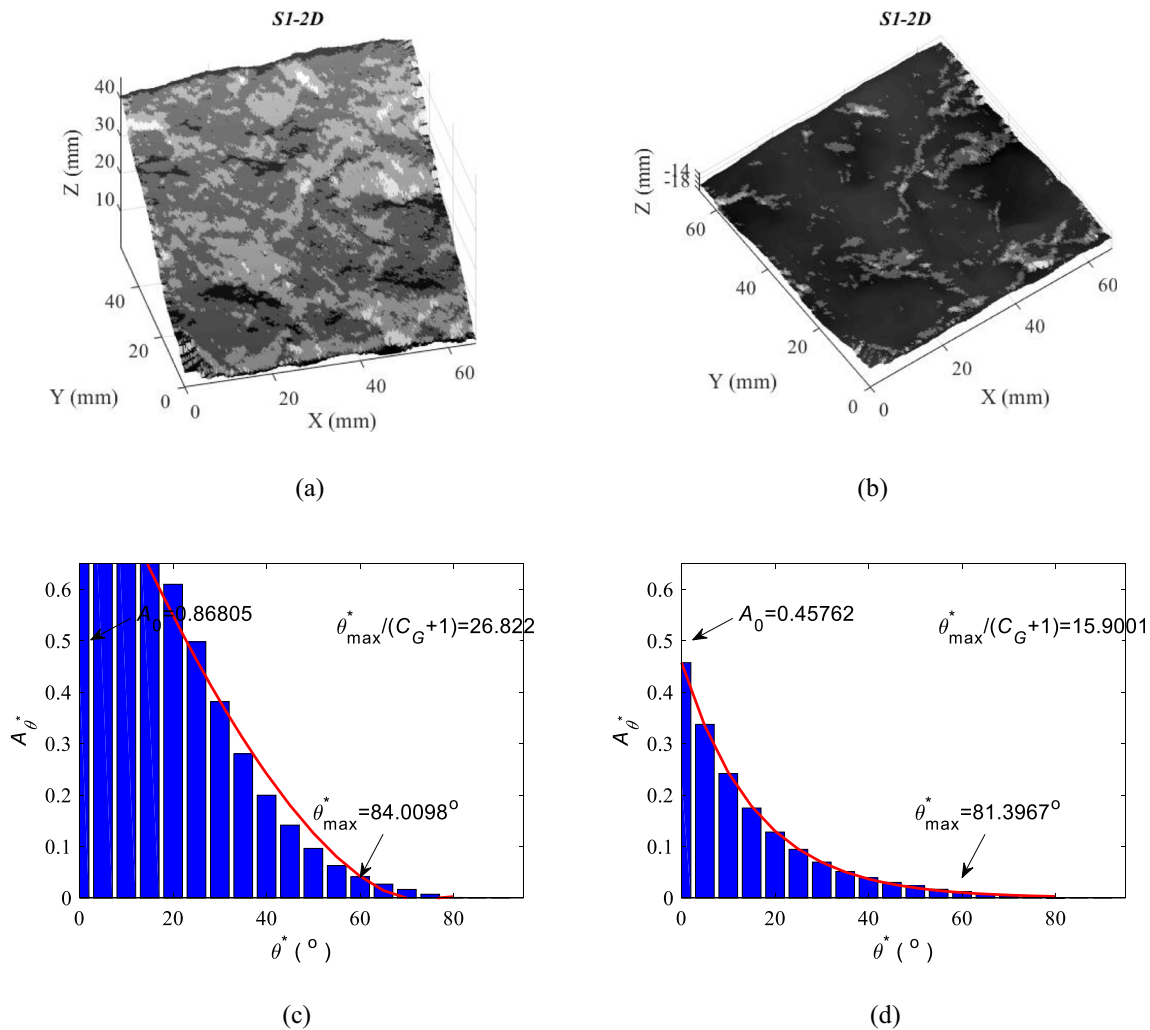


Fig. 9 Grayscale image generated based on the *BAP* method **a** before and **b** after removing the nonstationary features and A_{θ^*} vs. θ^* relational histograms and fitting curves based on the $\theta^*_{\max}/(C+1)$ method **c** before and **d** after removing the nonstationary features

coordinates specified by the distances of the corresponding points calculated in step (3).

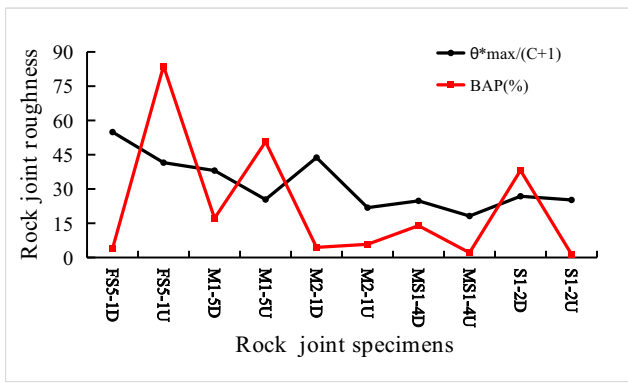
After implementing all of the above procedures, the original point clouds of rock joints were processed into a stationary data format, placing the point clouds on a horizontal plane (Fig. 8). Remarkably, rotation was performed only during the procedure of removing nonstationary features, and thus, no geometric characteristics, such as the amount of point, point density, or curvature, of the point clouds of rock joints were altered.

Results

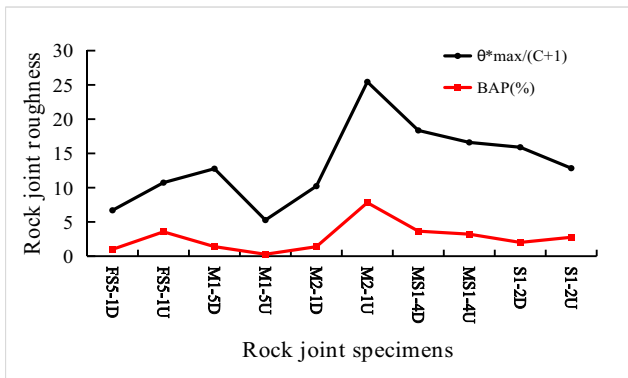
The *BAP* and $\theta^*_{\max}/(C+1)$ were determined both before and after removing the nonstationary features of point clouds to describe the roughness of the 10 rock joint specimens based

on the approaches mentioned in subsection 3.2, and the roughness evaluations using these two descriptors were compared. Since the roughness calculations are similar, for simplicity, this article presents only detailed information about the computational process for rock joint S1-2D, while the remaining samples are not presented in detail. Grayscale images of S1-2D were produced along the given analysis direction both before and after removing the nonstationary features (Fig. 9a, b), and the gray threshold was specified as 115 to extract the bright areas from the whole rock joint region using image segmentation to facilitate the *BAP* calculation. Additionally, the relation between A_{θ^*} and θ^* both before and after removing the nonstationary features was also established to estimate the $\theta^*_{\max}/(C+1)$ (Fig. 9c, d).

Accordingly, the two roughness indexes, the *BAP* and $\theta^*_{\max}/(C+1)$, were calculated based on the abovementioned methods for all specimens both before and after the removal of nonstationary features. Figure 10 a shows that the *BAP* and $\theta^*_{\max}/(C+1)$ vary significantly with the rock joint specimens;



(a)



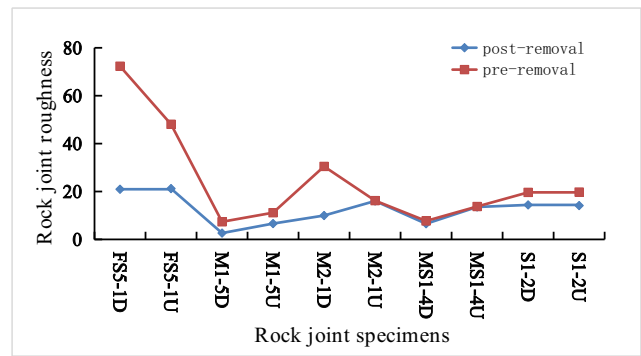
(b)

Fig. 10 Roughness evaluation based on the *BAP* and $\theta^*_{\max}/(C+1)$ with different rock joint specimens **a** before and **b** after removing nonstationary features

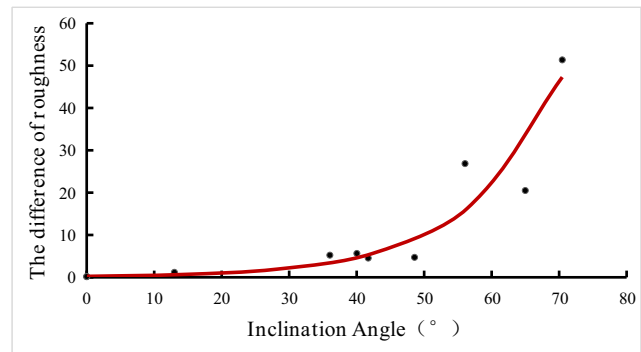
more importantly, different roughness variation trends are observed for the 10 specimens due to the presence of nonstationary features. In the *BAP* results, the roughest rock joint is FS5-1U with a *BAP* of 83.82%, while S1-2U has the minimum roughness with *BAP* of 1.40%. However, the maximum $\theta^*_{\max}/(C+1)$ is 54.92 for FS5-1D, and the minimum value is 18.16 for MS1-4U. By contrast, Fig. 10 b illustrates that the *BAP* has a similar tendency to $\theta^*_{\max}/(C+1)$ when both are computed based on point clouds without nonstationary features. M2-1U has the largest roughness with a *BAP* of 7.82% and a $\theta^*_{\max}/(C+1)$ value of 25.44, while M1-5U is characterized by the minimum roughness with a *BAP* of 0.38% and a $\theta^*_{\max}/(C+1)$ of 5.27. The *BAP* estimates closely match the $\theta^*_{\max}/(C+1)$ results, indicating that an accurate estimation of rock joint roughness can be obtained only through data without nonstationary features.

Discussion

To further study the effects of nonstationary features on the rock joint roughness assessment, the *JRC*, a widely used index, is introduced to describe the roughness of 10 specimens



(a)



(b)

Fig. 11 **a** Comparison between the *JRC* values from before and after removing nonstationary features and **b** the variability of the roughness difference with different inclination angles

based on 2D profiles. The *JRC* can be determined according to the parameter structure function (*SF*) (Tse and Cruden 1979):

$$JRC = -3.280 + 121.130\sqrt{SF} \tag{5}$$

A series of parallel profiles extracted from a 3D point cloud of a rock joint were utilized for the *SF* calculation to make the roughness estimation more robust:

$$SF = \frac{1}{M} \sum_{j=1}^M \left(\frac{1}{N-1} \sum_{i=1}^{N-1} (y_{i+1} - y_i)^2 dx \right) \tag{6}$$

where *M* is the total number of selected profiles, *N* is the total number of points in a profile, *dx* is the distance between two adjacent points, and *y_i* is the *y* axis of the *i*th point.

Figure 11 a illustrates that the inclination angle has a significant impact on the rock joint roughness. Furthermore, different trends are observed in the roughness assessment between the results from before and after removing nonstationary features, especially for the specimens FS5-1D, FS5-1U, and M2-1D. The pre- and post-removal roughness difference increases with the inclination angles of the rock joints, which is in good agreement with the above estimation at the 3D level (Fig. 11b).

Conclusions

To understand the influences of nonstationary features on rock joint roughness, high-density point clouds were collected from 10 specimens using a handheld laser scanner. Based on qualitative analysis, two 3D parameters, namely, the BAP and $\theta_{\max}^*/(C + I)$, were employed to evaluate the rock joint roughness estimates from before and after removing nonstationary features. The results show that the inclination angle, a nonstationary feature, has a significant effect on the estimated rock joint roughness, and the degree of this effect increases with the inclination angle. Therefore, the nonstationary features of rock joints should be removed when investigating rock joint roughness to improve the estimation accuracy. Furthermore, a simple but very effective method was proposed to remove the nonstationary features of rock joints based on the rotation and translation of coordinates; ultimately, the evaluation results without nonstationary features are consistent with the morphological observations.

Acknowledgments The authors are grateful to Liangqing Wang and Yi Cai for their help in data sampling and processing. Special thanks are owed to Yuhang Ren and Jenkins Wholda Teaway for their English language editing services. The authors also thank the editors and anonymous reviewers for their insightful and valuable suggestions.

Funding information This research was funded by the National Key R&D Program of China (No. 2017YFC1501303 & 2018YFC1507200) and the National Natural Science Foundation of China (No. 41602316).

References

- Babanouri N, Nasab SK, Sarafrazi S (2013) A hybrid particle swarm optimization and multi-layer perceptron algorithm for bivariate fractal analysis of rock fractures roughness. *Int J Rock Mech Min Sci* 60(60):66–74. <https://doi.org/10.1016/j.ijmms.2012.12.028>
- Barton N (1973) Review of a new shear-strength criterion for rock joints. *Eng Geol* 7(4):287–332. [https://doi.org/10.1016/0013-7952\(73\)90013-6](https://doi.org/10.1016/0013-7952(73)90013-6)
- Barton N, Choubey V (1977) The shear strength of rock joints in theory and practice. *Rock Mech Rock Eng* 10(1–2):1–54. <https://doi.org/10.1007/BF01261801>
- Belem T, Etienne FH, Souley M (2000) Quantitative parameters for rock joint surface roughness. *Rock Mech Rock Eng* 33(4):217–242. <https://doi.org/10.1007/s006030070001>
- Bitenc M, Kieffer DS, Khoshelham K (2016) Evaluation of wavelet and non-local mean denoising of terrestrial laser scanning data for small-scale joint roughness estimation. *ISPRS-International Archives of the Photogrammetry Remote Sensing and Spatial Information Sciences*. <https://doi.org/10.5194/isprsarchives-XLI-B3-181-2016>
- Clark KC (1986) Computation of the fractal dimension of topographic surfaces using the triangular prism surface area method. *Comput Geosci* 12(5):713–722. [https://doi.org/10.1016/0098-3004\(86\)90047-6](https://doi.org/10.1016/0098-3004(86)90047-6)
- Du SG, Tang HM (1993) A study on the anisotropy of joint roughness coefficient in rock mass. *J Eng Geol* 1:32–42
- Ge YF, Kulatilake PHSW, Tang HM, Xiong C (2014) Investigation of natural rock joint roughness. *Comput Geotech* 55(55):290–305. <https://doi.org/10.1016/j.compgeo.2013.09.015>
- Ge YF, Tang HM, Eldin MAME, Chen PY, Wang LQ, Wang JG (2015) A description for rock joint roughness based on terrestrial laser scanner and image analysis. *Sci Rep* 5:16999. <https://doi.org/10.1038/srep16999>
- Ge YF, Tang HM, Eldin MA, Wang LQ (2017) Evolution process of natural rock joint roughness during direct shear tests. *International Journal of Geomechanics* 17(5). [https://doi.org/10.1061/\(ASCE\)GM.1943-5622.0000694](https://doi.org/10.1061/(ASCE)GM.1943-5622.0000694)
- Ge YF, Tang HM, Xia D, Wang LQ, Zhao BB, Teaway JW, Chen HZ, Zhou T (2018) Automated measurements of discontinuity geometric properties from a 3D-point cloud based on a modified region growing algorithm. *Eng Geol* 242:44–54. <https://doi.org/10.1016/j.enggeo.2018.05.007>
- Grasselli G, Egger P (2003) Constitutive law for the shear strength of rock joints based on three-dimensional surface parameters. *Int J Rock Mech Min Sci* 40(1):25–40. [https://doi.org/10.1016/S1365-1609\(02\)00101-6](https://doi.org/10.1016/S1365-1609(02)00101-6)
- Jiang Q, Feng XT, Gong YH, Song LB, Ran SG, Cui J (2016) Reverse modelling of natural rock joints using 3D scanning and 3D printing. *Comput Geotech* 73:210–220. <https://doi.org/10.1016/j.compgeo.2015.11.020>
- Khoshelham K, Altundag D, Ngan-Tillard D, Menenti M (2011) Influence of range measurement noise on roughness characterization of rock surfaces using terrestrial laser scanning. *International Journal of Rock Mechanics and Mining Sciences* 48(8):1215–1223. <https://doi.org/10.1016/j.ijmms.2011.09.007>
- Kulatilake PHSW, Shou G, Huang TH, Morgan RM (1995) New peak shear strength criteria for anisotropic rock joints. *International Journal of Rock Mechanics and Mining Sciences and Geomechanics Abstracts* 32(7):673–697. [https://doi.org/10.1016/0148-9062\(95\)00022-9](https://doi.org/10.1016/0148-9062(95)00022-9)
- Kulatilake PHSW, Balasingam P, Park J, Morgan RM (2006) Natural rock joint roughness quantification through fractal techniques. *Geotech Geol Eng* 24(5):1181–1202. <https://doi.org/10.1007/s10706-005-1219-6>
- Li YC, Wu W, Li B (2018) An analytical model for two order asperity degradation of rock joints under constant normal stiffness conditions. *Rock Mech Rock Eng* 1:1–15. <https://doi.org/10.1007/s00603-018-1405-5>
- Luo ZY, Du SG, Huang M (2015) An experimental study of size effect of roughness coefficient on rock joint using push-pull apparatus. *Rock Soil Mech* 36(12):3381–3386. <https://doi.org/10.16285/j.rsm.2015.12.006>
- Ma YX, Guo YL, Lei YJ, Lu M, Zhang J (2017) Efficient rotation estimation for 3D registration and global localization in structured point clouds. *Image Vis Comput* 67:52–66. <https://doi.org/10.1016/j.imavis.2017.09.003>
- Maerz NH, Franklin JA, Bennett CP (1990) Joint roughness measurement using shadow profilometry. *International Journal of Rock Mechanics and Mining Sciences and Geomechanics Abstracts* 27(5):329–343. [https://doi.org/10.1016/0148-9062\(90\)92708-M](https://doi.org/10.1016/0148-9062(90)92708-M)
- Mah J, McKinnon SD, Samson C, Thibodeau D (2016) Wire mesh filtering in 3D image data of rock faces. *Tunnelling and Underground Space Technology* 52(10):111–118. <https://doi.org/10.1016/j.tust.2015.11.005>
- Mlynarczuk M (2010) Description and classification of rock surfaces by means of laser profilometry and mathematical morphology. *Int J Rock Mech Min Sci* 47(1):138–149. <https://doi.org/10.1016/j.ijmms.2009.09.004>
- Nizametdinov FK, Nagibin AA, Levashov VV, Nizametdinov RF, Nizametdinov NF, Kasymzhanova AE (2016) Methods of in situ strength testing of rocks and joints. *J Min Sci* 52(2):226–232. <https://doi.org/10.1134/S1062739116020357>
- Odling NE (1994) Natural fracture profiles, fractal dimension and joint roughness coefficients. *Rock Mech Rock Eng* 27(3):135–153. <https://doi.org/10.1007/BF01020307>

- Tang HM, Wasowski J, Juang CH (2019) Geohazards in the three Gorges Reservoir Area, China-Lessons learned from decades of research. *Eng Geol* 261:105267. <https://doi.org/10.1016/j.enggeo.2019.105267>
- Tatone BSA, Grasselli G (2009) A method to evaluate the three-dimensional roughness of fracture surfaces in brittle geomaterials. *Rev Sci Instrum* 80(12):125110. <https://doi.org/10.1063/1.3266964>
- Tatone BSA, Grasselli G (2010) A new 2D discontinuity roughness parameter and its correlation with JRC. *Int J Rock Mech Min Sci* 47(8):1391–1400. <https://doi.org/10.1016/j.ijrmms.2010.06.006>
- Tse R, Cruden DM (1979) Estimating joint roughness coefficients. *International Journal of Rock Mechanics and Mining Sciences and Geomechanics Abstracts* 16(5):303–307. [https://doi.org/10.1016/0148-9062\(79\)90241-9](https://doi.org/10.1016/0148-9062(79)90241-9)
- Turk N, Greig MJ, Dearman WR, Amin FF (1987) Characterization of rock joint surfaces by fractal dimension. *The 28th U.S. Symposium on Rock Mechanics* 28:1223–1236
- Wu TH, Ali EM (1978) Statistical representation of joint roughness. *International Journal of Rock Mechanics and Mining Sciences and Geomechanics Abstracts* 15(5):259–262. [https://doi.org/10.1016/0148-9062\(78\)90958-0](https://doi.org/10.1016/0148-9062(78)90958-0)
- Xie HP, Wang JA, Stein E (1998) Direct fractal measurement and multifractal properties of fracture surface. *Phys Lett A* 242:41–50. [https://doi.org/10.1016/s0375-9601\(98\)00098-x](https://doi.org/10.1016/s0375-9601(98)00098-x)
- Yu XB, Vayssade B (1991) Joint profiles and their roughness parameters. *International Journal of Rock Mechanics and Mining Sciences and Geomechanics Abstracts* 28(4):333–336. [https://doi.org/10.1016/0148-9062\(91\)90598-G](https://doi.org/10.1016/0148-9062(91)90598-G)